A High-Fidelity Level-Set Flamelet Approach for Predicting Turbulent Reacting Flows

Cosmin Safta,[*] Foluso Ladeinde,[†] Xiaodan Cai[‡], and Kehinde Alabi,[§]
Thaerocomp Technical Corporation, P.O. Box 1527, Stony Brook, NY 11790-0609

An approach to predict partially-premixed turbulent reacting flows is presented in this paper within the context of large-eddy simulation (LES). A high-order, fully compressible LES flow solver is combined with a level-set/mixture fraction flamelet formulation to predict combustion in premixed and partially-premixed turbulent reacting flows. The non-reacting and reacting results for a V-gutter flame holder and a lean premixed dump combustor are compared with available experimental results and previous numerical studies. The combined level-set/mixture fraction approach is validated by the good agreement between the numerical results and the experimental data observed for both configurations.

I.   Introduction

Modern propulsion systems are required to reduce NOx emissions for environmental reasons. While a number of approaches have been investigated for lowering pollutant emissions, lean-premixed combustion (LPM) is considered an effective and competitive means to achieve this goal.[1] However, lean combustors operate in a partially-premixed flame regime and are prone to combustion instabilities that may reach sufficient amplitudes to interfere with the operation of the propulsion system. The large-eddy simulation (LES) approach received increased attention from the combustion research community in recent years due to its potential to accommodate realistic engineering configurations and, unlike the Reynolds-Averaged Navier Stokes (RANS) methods, accurately predict non-universal turbulent flow features. The aim of the numerical studies is to improve the understanding of the turbulence-chemistry interactions in complex configurations and to result in improved designs for future combustors.

Several approaches have been proposed for the treatment of premixed flames within the context of LES. In the present study, we consider the level-set method which attempts to model the premixed flame from a geometrical point of view. The level-set or G-equation, originally proposed by Williams,[2] models the evolution of the flame front. Peters[3] proposed a transport equation for the level-set function treated as a distance function within the context of RANS. This approach was used by Nilsson and Bai[4] who also considered the effects of flame stretch in their flamelet model. Pitsch and Duchamp de Lageneste[5] and Pitsch,[6] using LES, extended the level-set approach to include both the thin and corrugated flame regimes. Their numerical approach was based on a second-order spatial scheme an improved model for the turbulent burning velocity. The mixing between the combustion products and the surrounding inert flow field was also modeled. Huang et al.[7] considered the level-set approach and LES to study the combustion dynamics in a lean-premixed swirl-stabilized combustor. The LES equations were solved with a second-order finite volume method while a flamelet library based on freely propagating premixed flames was generated.

In the present work, we combine the level-set approach for premixed flame configurations with the conserved variable approach for non-premixed configurations. The combined model is similar to the approach used by Duchamp de Lageneste and Pitch[8] for a low-Mach number formulation. In the present work, the combustion model is based on a compressible formulation. The ability of the model to capture partially-premixed flame characteristics is established by comparing the calculated results with those from available experiments.

The computational procedure in the present work is based on high-order spatial discretization of the governing equations. The compact, Padé approximant procedure[9] is used for low Mach number flows and the weighted essentially non-oscillatory scheme[10] (WENO) for high Mach number flows. Thus, high-fidelity simulation is available at all speeds, from incompressible to supersonic or even hypersonic speeds. The high-order spatial discretization is marched in time by a fourth-order Runge-Kutta integration procedure. The node-implicit approach

---

[*] Research Engineer, AIAA Member.

[†] Director of Research, AIAA Life Member and Associate Fellow.

[‡] Senior Research Engineer, AIAA Member.

[§] Research Engineer, AIAA Member.

of Beam and Warming[11] is also supported for time integration. In order to accommodate the analysis of realistic problems with complicated geometries and be competitive with unstructured mesh methods, a matching high-order overset procedure was also developed and implemented.

II.   The Mathematical Models and Numerical Procedures

The transport equations for the filtered flow field variables, including those associated with combustion, are presented in this section, as are the numerical procedures for the spatial and temporal discretization of the transport equations.

A. The Governing Equations

The fully compressible forms of the continuity, momentum and energy equations are employed in this study since we are interested in the non-linear coupling between the acoustic, vorticity, and combustion fields. The Favre-averaged equations are written in conservation form:[7]

$$\frac{\partial \overline{\rho}}{\partial t} + \frac{\partial \left(\overline{\rho} \tilde{u}_j \right)}{\partial x_j} = 0,$$

$$\frac{\partial \left(\overline{\rho} \tilde{u}_i \right)}{\partial t} + \frac{\partial \left(\overline{\rho} \tilde{u}_i \tilde{u}_j + \overline{p} \delta_{ij} \right)}{\partial x_j} = \frac{\partial \left(\tau_{ij} - \tau_{ij}^{SGS} \right)}{\partial x_j},$$

$$\frac{\partial \left(\overline{\rho} \tilde{E} \right)}{\partial t} + \frac{\partial \left(\left(\overline{\rho} \tilde{E} + p \right) \tilde{u}_j \right)}{\partial x_j} = \frac{\partial \left(\tilde{u}_i \tau_{ij} - q_j + H_j^{SGS} + \sigma_j^{SGS} \right)}{\partial x_j}. \tag{1}$$

Here, $\overline{\rho}$ is the mass density, $\tilde{u}_i$ are the velocity components in the physical coordinate directions, and $\tilde{E}$ is the total specific energy. Note that in Eq. (1), an overline on a variable implies Reynolds-averaging, while a tilde denotes Favre-averaging. In LES, the large scale motions are fully-resolved while the effects of the small scales on the large ones are modeled. The separation between the large and small scales is determined by the grid size, Δ. In the system of transport equations (1), the filtered viscous stress tensor, τ_{ij}, and the heat flux vector, q_i, are based on the filtered flow variables. The sub-grid scale (SGS) terms, representing the effects of the small scale structures on the resolved scales, are

$$\tau_{ij}^{SGS} = \overline{\rho u_i u_j} - \overline{\rho} \tilde{u}_i \tilde{u}_j, \quad \sigma_j^{SGS} = \overline{u_i \tau_{ij}} - \tilde{u}_i \overline{\tau_{ij}},$$

$$H_i^{SGS} = \overline{\rho E u_i} - \overline{\rho} \tilde{E} \tilde{u}_i + \overline{p u_i} - \overline{p} \tilde{u}_i. \tag{2}$$

The unclosed viscous work, σ_j^{SGS}, is assumed to be small and is neglected in the present work. The SGS contribution to the shear stresses, τ_{ij}^{SGS}, is computed using the Smagorinsky model.[12] The model parameters are determined empirically, or are dynamically computed as a function of the local flow conditions, using the formulation of Germano et al.[13] and Moin et al.,[14] with the modifications proposed by Lilly.[15] The SGS energy flux, H_i^{SGS}, is modeled as

$$H_i^{SGS} = -\overline{\rho} \frac{\nu_t}{Pr_t} \left(\frac{\partial \tilde{h}}{\partial x_i} + \tilde{u}_j \frac{\partial \tilde{u}_j}{\partial x_i} + \frac{1}{2} \frac{\partial k^{SGS}}{\partial x_i} \right). \tag{3}$$

Here, $\tilde{h}$ is the filtered specific enthalpy, Pr_t is the turbulent Prandtl number, and k^{SGS} is the kinetic energy contained in the sub-grid scales.

The filtered total specific energy is given as

$$\tilde{E} = \int_{T_0}^{\tilde{T}} c_p dT - \frac{\overline{p}}{\overline{\rho}} + \frac{\tilde{u}_j \tilde{u}_j}{2} + k^{SGS} + \tilde{H}_f^0. \tag{4}$$

Note that the Favre-filtered formation enthalpy in Eq. (4), $\tilde{H}_f^0$, accounts for the contribution of chemical reactions to the specific total energy, $\tilde{E}$. This term is computed through a flamelet library as outlined in Section II.B.

Spatial Discretization and Temporal Integration

In order to facilitate the numerical simulation of flow configurations around arbitrary complicated bodies, the transport equations need to be re-cast in the form of a generalized curvilinear coordinate system. These equations are implemented in AEROFLO, which is a multidisciplinary CFD software product developed by Thaerocomp Technical Corp. Various high-order and low-order numerical schemes are available in this code for the discretization of Eq. (1). For low speed flows, a sixth-order accurate compact scheme is used. For high-speed flows, a fifth-order accurate WENO scheme is employed. For numerical simulations using lower quality grids, a robust second-order MUSCL scheme is implemented. The details of the implementation of these schemes are presented elsewhere.[16]

Due to the strong interaction between the flow field and the flame, accurate time-dependent solutions are required. To obtain this, either a second-order Beam and Warming algorithm[11] or the classical fourth-order Runge-Kutta scheme in its low-storage form[17] are employed for time integration of Eq. (1).

B. The Laminar Flamelet Approach

In order to analyze premixed and partially-premixed reacting flows of practical interest, we couple the compressible formulation for the transport of mass, momentum, and energy, presented in the previous section, with a level-set methodology for premixed combustion. The level-set formulation is also augmented with a mixture fraction approach for non-premixed combustion. The combined model allows the modeling of premixed flames with variable equivalence ratios, and is a building block for the modeling of flames in configurations that encompass all regimes: premixed, non-premixed, and partially-premixed. The level-set methodology is outlined in Section II.C. The mixture fraction approach is described in Section II.D.

The main idea behind the flamelet approach, which is used to calculate the effects of chemical heat release on the flow field, is the assumption that a turbulent flame is a collection of laminar flamelets embedded in an otherwise inert turbulent flow. The flame inner structure can be calculated independent of the turbulent flow, using arbitrary detailed kinetic models and realistic multi-species transport properties. The filtered formation enthalpy, $\tilde{H}_f^0$ in Eq. (4), is computed as

$$\tilde{H}_f^0 = \int H_f^0(y_1, y_2, \ldots, y_n) PDF(y_1, y_2, \ldots, y_n) dy_1 dy_2 \ldots dy_n , \qquad (5)$$

where $y_1, y_2, \ldots, y_n$, are independent variables for the flamelet model. The laminar formation enthalpy at T_0, H_f^0, is defined as

$$H_f^0 = \sum_{i=1}^{N_s} Y_i \Delta h_{f,i}^0 , \qquad (6)$$

where Y_i is the molar reaction rate of species i, $\Delta h_{f,i}^0$ is the enthalpy of formation of species i, and N_s is the total number of species in the kinetic model. The reference temperature, T_0 (also used in the definition of total energy, Eq. (4)), is configuration-dependent and is usually set to the temperature of the main incoming premixed or non-premixed stream.

The freely-propagating premixed flame and the opposed-jet flame are two canonical configurations that are widely used to generate model data for flamelet libraries. For these configurations, the flame structure is assumed to be one-dimensional, which leads to some simplifications of the multi-species transport equations. The governing equations are given elsewhere.[18,19] The freely-propagating flame configuration is used to determine the laminar flame velocity, $S_{L,0}$, and to generate stretch-free premixed flame data (species mass fractions and reaction rate profiles, etc.) for various values of the fuel-to-oxidizer equivalence ratio, Φ, and reference ambient pressures. In the second configuration, a stretched flame is formed between two opposing jets. Depending on the jets' mixture set-up, the flame can be premixed, non-premixed, or partially-premixed. The flame stretch or strain rates are controlled by adjusting the velocities of the opposing jets.

The flamelet library is constructed by tabulating the filtered source term, $\tilde{H}_f^0$, as a function of G and K for a range of values of Φ (or mixture fraction, Z), variance of Z, and computational grid size, Δ. Here, G is the distance to the flame surface, and K is the flame stretch rate. The shapes of various PDF's used to compute these libraries are given in the following sections.

C. The Level-Set Equation

The evolution of Favre-averaged G, or $\tilde{G}$, is modeled by a level-set equation:[3]

$$\frac{\partial(\overline{\rho}\tilde{G})}{\partial t} + \frac{\partial(\overline{\rho}\tilde{u}_i\tilde{G})}{\partial x_i} = \overline{\rho}S_T\left|\frac{\partial\tilde{G}}{\partial x_i}\right| - \overline{\rho}D_t\tilde{\kappa}\left|\frac{\partial\tilde{G}}{\partial x_i}\right|,$$

(7)

where S_T is the turbulent burning velocity, D_t is the turbulence diffusivity, $D_t = \nu_t / Pr_t$, and $\tilde{\kappa}$ is the curvature of the flame surface, $\tilde{\kappa} = \nabla \cdot \left(-\nabla\tilde{G}/\left|\nabla\tilde{G}\right|\right)$. The turbulent flame velocity is modeled as[6]

$$\frac{S_T - S_L}{S_L} = -\frac{b_3^2}{2b_1}\frac{Pr}{Sc_t}\frac{\nu_t}{\nu}\frac{S_L}{u'_\Delta} + \sqrt{\left(\frac{b_3^2}{2b_1}\frac{Pr}{Sc_t}\frac{\nu_t}{\nu}\frac{S_L}{u'_\Delta}\right)^2 + b_3^2\frac{Pr\,\nu_t}{Sc_t\nu}}.$$

(8)

Here Pr is the laminar Prandtl number, Sc_t is the turbulence sub-grid Schmidt number, ν and ν_t are the laminar and turbulent kinematic viscosities, respectively, S_L is the laminar flame velocity, and u'_Δ is the sub-grid velocity fluctuation. The values of the constants b_1 and b_3 are taken from Peters:[3] $b_1 = 2$ and $b_3 = 1$, while Sc_t is set to 0.4.[20]

High-order ENO discretization[21-23] is used to evaluate the spatial derivates in Eq. (7), with local Lax-Friedrichs flux-splitting, to ensure a robust evaluation of the convection term in this equation. Time integration is based on second- and third-order TVD Runge-Kutta schemes.

Equation (7) is valid only at the flame front, $\tilde{G} = 0$. Since the distance function property of $\tilde{G}$ is not preserved by the level-set equation, this condition needs to be enforced through a re-initialization procedure. For this purpose, we use the procedure of Sussman et al.[24] with the extension in Russo and Smereka.[25] This procedure involves solving the following equation to steady state:

$$\frac{\partial G}{\partial \tau} = \text{sgn}(G_0)(1 - |\nabla G|), \quad G(x,0) = G_0(x).$$

(9)

Here, $\text{sgn}(\cdot)$ is the sign function. Note that the tilde on top of the variable G has been dropped for simplicity. Due to the hyperbolic nature of Eq. (9), the characteristics propagate outward from the zero level, $G = 0$. Since the flame thickness is small compared to the large scale structures, Eq (9) is driven to steady state only for a limited region around the flame surface. The narrow band method[16] has been implemented to ensure the computational efficiency of the re-initialization procedure. The discretization method for equation (9) is based on that of Sussman et al.[24] The procedure, described in detail in Safta et al.,[26] was generalized for a curvilinear coordinate system.

The PDF, $P(G,Z,K)$, for the formation enthalpy depends on the flame distance, G, the mixture fraction, Z, and the stretch rate, K. Assuming statistical independence, $P(G,Z,K)$ is taken to be a product of a Gaussian distribution for the flame distance function,[7] a beta-distribution for the mixture fraction, and a log-normal distribution for the flame stretch rate.[27] This model can account for variable equivalence ratios and partial extinction of the turbulent flame when the local stretch rate becomes larger than the extinction limit, K_{ext}. The PDF for G is given by

$$PDF(G;x,t) = \frac{1}{\sqrt{2\pi\overline{G_0''^2}}}\exp\left(-\frac{\left(G - \tilde{G}(x,t)\right)^2}{2\overline{G_0''^2}}\right),$$

(10)

where $\overline{G_0''^2}$ is the conditional variance at the flame front and $\tilde{G}(x,t)$ is the signed distance to the flame front around which the source term is filtered. The variance of G, which is also the turbulent flame thickness, can be computed via a transport equation or simply modeled based on dimensional analysis. Here, the approach by Yang and coworkers[7] is adopted:

$$\sqrt{\overline{G_0''^2}} \equiv l_{F,t} = l_F + \Delta,$$

(11)

where $l_{F,t}$ is the turbulent flame thickness, l_F is the laminar flame thickness and Δ is the grid size. A log-normal distribution is assumed for the flame stretch:

$$PDF(K) = \frac{1}{\sqrt{2\pi}K\sigma}\exp\left(-\frac{(\ln K - \mu)^2}{2\sigma^2}\right),$$

$$\mu = \frac{1}{2}\left(\ln\frac{\varepsilon}{3\nu} - 2\sigma^2\right) - \ln 2$$

(12)

where $\sigma^2 = 0.34$ and ε is the dissipation of the sub-grid fluctuations.

The PDF of the mixture fraction is given in the next section.

D. Mixture Fraction Formulation

In order to model a partially-premixed combustion process, a transport equation for a conserved scalar is solved in addition to the equation for the level-set function. The conserved scalar is analogous to the mixture fraction used in non-premixed combustion studies. This scalar is related to the fuel-to-oxidizer equivalence ratio, Φ, as

$$Z = \frac{\Phi}{\left(\Phi + \dfrac{1 - Z_{st}}{Z_{st}}\right)}. \tag{13}$$

By convention, the conserved scalar, Z, will be called mixture fraction throughout the rest of the paper, and Z_{st} is its stoichiometric value, which occurs when $\Phi = 1$. The filtered LES equation for the Favre-filtered mixture fraction is written as[8]

$$\frac{\partial(\bar{\rho}\tilde{Z})}{\partial t} + \frac{\partial(\bar{\rho}\tilde{u}_i\tilde{Z})}{\partial x_i} = \frac{\partial}{\partial x_j}\left[(\tilde{\alpha}_Z + \alpha_t)\frac{\partial \tilde{Z}}{\partial x_j}\right]. \tag{14}$$

The laminar and turbulent diffusivities for the mixture fraction are set equal to the respective values used for the temperature:

$$\tilde{\alpha}_Z = \frac{\mu}{\mathrm{Pr}}, \alpha_t = \frac{\mu_t}{\mathrm{Pr}_t}. \tag{15}$$

The mixture fraction PDF is modeled with a two parameter beta distribution:

$$\tilde{P}(Z;a,b) = Z^a (1 - Z)^b \frac{\Gamma(a+b)}{\Gamma(a)\Gamma(b)}, \tag{16}$$

where Γ is the Euler gamma function, and a, b are constants defined by

$$a = \tilde{Z}\left(\frac{\tilde{Z}(1-\tilde{Z})}{\overline{Z''^2}} - 1\right), \quad b = (1-\tilde{Z})\left(\frac{\tilde{Z}(1-\tilde{Z})}{\overline{Z''^2}} - 1\right). \tag{17}$$

Here, $\tilde{Z}$ is the mixture fraction around which the flame data is filtered and $\overline{Z''^2}$ is its variance. In the numerical simulations, $\overline{Z''^2}$ is computed using the scale-similarity model of Cook and Riley.[28]

III.   Results

The numerical procedures described in the previous section have been implemented into AEROFLO. The aim of the combined high-order LES/level-set/mixture fraction approach is to accurately predict transient flame phenomena for partially-premixed flames and the detailed coupling between flow and combustion instabilities. The results presented here correspond to premixed flames with uniform and variable equivalence ratios.

A. Flamelet Library

The laminar flame data used in our flamelet library was validated in our previous work[26] against experimental results and the predictions from the well-established Chemkin II software.[18,19,29] Sample filtered formation enthalpy ($\tilde{H}_f^0$) data is shown in Fig. 1. These results correspond to premixed flames for which the presumed PDF's are described in Sections II.C and II.D. In this figure, $G = 0$ corresponds to the flame surface, defined as the location of the peak heat release rate. The filtering process results in a multidimensional table such that the filtered formation enthalpy is a function of the distance to the flame surface, equivalence ratio (through the mixture fraction), grid size, mixture fraction variance, and flame stretch rate.

In order to save computational resources, the flamelet library is constructed prior to the start of the LES simulation. The range of values for each independent variable is chosen according to the values of characteristic parameters for the numerical simulation. The values for the signed distance to the flame are set large enough to ensure the entire flame is contained in the table. The set of equivalence ratio values covers the range [Φ_{min}, Φ_{max}] corresponding to the experimental conditions, while the stretch rate values are set in the range [$0, K_{ext}$], where K_{ext} is the extinction strain rate. The grid size, Δ, and mixture fraction variance, $\overline{Z''^2}$, become independent variables for

the flamelet library since they appear as parameters in the PDFs for G and Z. Solutions are generated for several grid size values, $\Delta_{min} < \Delta < \Delta_{max}$, and mixture fraction variance values, $0 < \dfrac{\overline{Z''^2}}{\widetilde{Z}(1-\widetilde{Z})} < 1$. Here, Δ_{min} and Δ_{max} are the minimum and maximum grid sizes, respectively, for a computational mesh. During the simulation, the values of the filtered formation enthalpy are extracted from the flamelet table through a multi-dimensional linear interpolation. The interpolation algorithm is designed to accommodate tables based on arbitrary numbers of independent variables. The procedure adapts automatically to cases where one or more independent variables are neglected (e.g. flame with constant equivalence ratio and/or $K=0$).

The results shown in Fig. 1 correspond to stretch-free, $K=0$, methane-air flames computed using the detailed kinetic model GRI-Mech 3.0.[30] The peak negative formation enthalpy occurs near the stoichiometric mixture fraction value which corresponds to $\widetilde{Z} \approx 0.055$. The grid size, Δ, affects the width of the Gaussian PDF in Eq. (10) through the model for the turbulent flame thickness in Eq. (11). Since Δ is larger for the results shown in Fig. 1(b) compared to Fig. 1(a), the slope of the formation enthalpy surface between fresh ($G<0$) and burnt ($G>0$) regions is smaller, and the numerical flame thickness increases because of a poorer resolution at the flame front. The values of
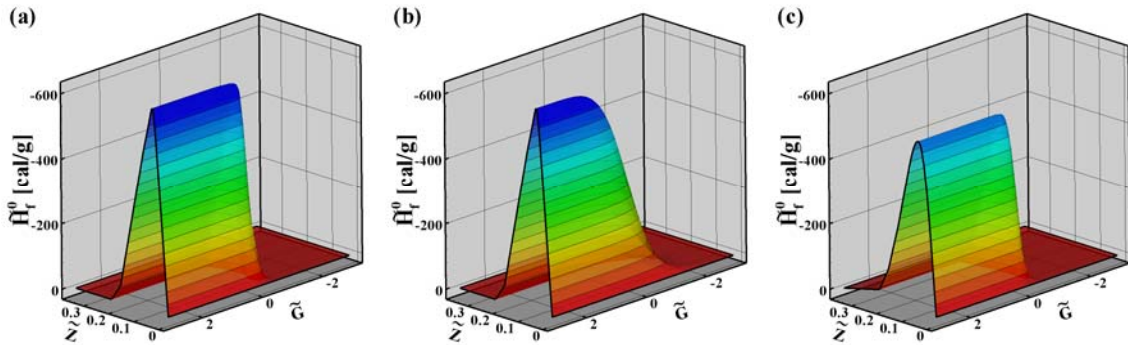
Fig. 1 Sample $\widetilde{H}_f^0$ values for methane-air flame at various values of the equivalence ratio. The filter width in the G-direction corresponds to $\dfrac{\Delta}{L_{ref}} = 0.003$ for (a) and (c) and to $\dfrac{\Delta}{L_{ref}} = 0.1$ for (b). For (a) and (b) the mixture fracture variance is $\dfrac{\overline{Z''^2}}{\widetilde{Z}(1-\widetilde{Z})} = 10^{-4}$, while for (c), $\dfrac{\overline{Z''^2}}{\widetilde{Z}(1-\widetilde{Z})} = 10^{-2}$. For this configuration $L_{ref}=3cm$ and $K=0$.
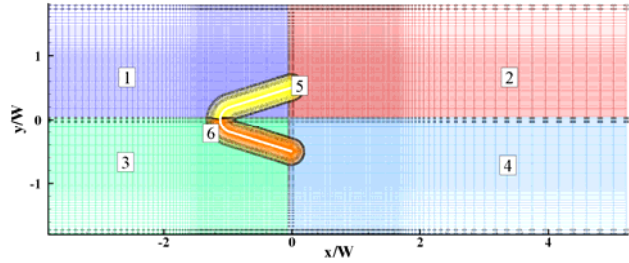
the mixture fraction variance have a similar effect in the mixture fraction, $\widetilde{Z}$, direction.

## B. LES of a V-Gutter Flame Holder

The flow around a V-gutter flame holder is used to test the capability of the level-set flamelet approach for premixed flames with fixed equivalence ratio. A six-block overset computational grid used for numerical simulations of a two-dimensional V-gutter flame holder model is shown in Fig. 2. The total number of grid points in the computational domain is approximately 45,000. The flame holder traverses the height of the test section (*z*-direction not shown in the figure). The two-dimensional model is assumed to be located at the center of the test rig.

The numerical details are presented elsewhere.[26] In this section, the non-reacting and reacting flow results are compared to available experimental data and results from previous numerical studies. To our knowledge this is the first LES simulation of the V-gutter flame holder. The Reynolds number based on the inflow streamwise velocity and the V-gutter width is 29,000 and the Mach number is 0.15 for both the non-reacting and the reacting simulations.

Snapshots of the vorticity fields for the non-reacting and reacting simulations are shown in Fig. 3. In Fig. 3(a), two dominant vortex structures can be seen. The large-scale structures are the von Karman vortices typical of the shedding behind a bluff-body. There are also trails of smaller vortices that originate from the trailing edge of the V-gutter. The rotation of the large vortices results in a boundary layer that grows on the inside surfaces of the v-gutter. The inner boundary layer meets with the outer boundary layer at the trailing edge of the V-gutter and a secondary shedding process develops. The small vortices that develop at the

Fig. 2 Computational domain for the v-gutter simulations.

V-gutter trailing edges are convected with the large structures and are quickly dissipated into elongated vortex structures.

(a)   (b)
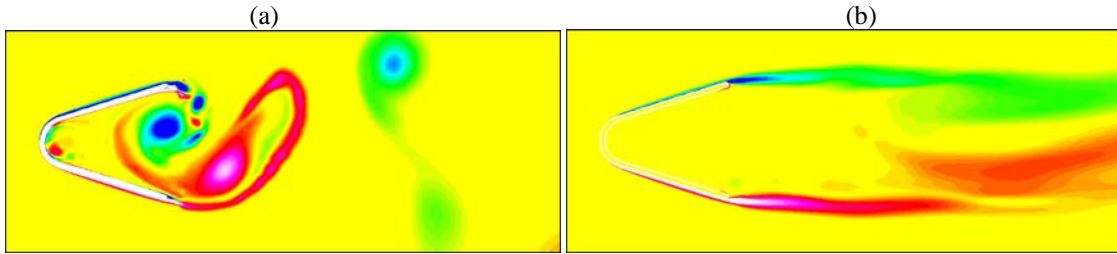
Fig. 3 A vorticity field snapshot: (a) non-reacting simulation and (b) reacting simulation.

The heat released by the flame that forms downstream of the V-gutter leads to different flow dynamics in the reacting case relative to the non-reacting case. For the reacting flow, the von Karman vortex shedding is suppressed and the vorticity field shown in Fig. 3(b) is characterized by two elongated vortical structures that originate from the V-gutter trailing edges. Further downstream, the shear layers become more unstable and asymmetric vortices are generated. The vortex dynamics observed here for the non-reacting and reacting LES results is consistent with previous experimental results for a similar configuration.[31]

(a)   (b)
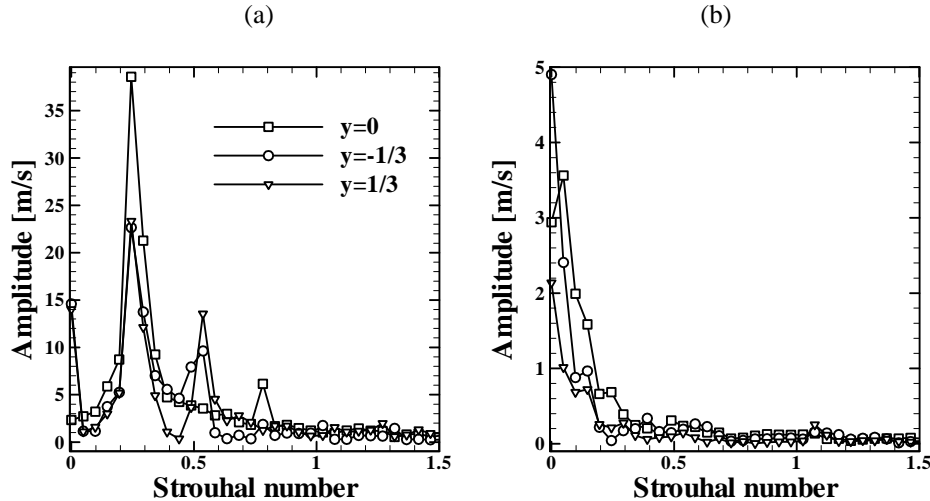
Fig. 4 Dominant shedding frequencies for the V-gutter flame holder at three cross-wise locations at 1/3 V-gutter widths downstream of the flame holder: (a) non-reacting simulation, (b) reacting simulation.

In order to determine the shedding frequency for the two sets of results, the transverse velocity signals are examined at several locations in the wake of the v-gutter. Fig. 4 presents the FFT of the LES velocity data 1/3 of a V-gutter width downstream of the flame holder and at three positions across the wake. For the non-reacting simulation, all centerline and off-centerline signals exhibit a dominant frequency corresponding to a Strouhal number, $St=0.24$. This value is slightly lower than that for the experiments[26] which report a value of $St=0.32$. Three dimensional numerical studies will be conducted to determine the source of this discrepancy. The FFT analysis of the velocity signals for the reacting case confirms the visual observation for suppression of the vortex shedding in the wake of the flame holder. For this case, the amplitude range of the velocity signal is much smaller compared to its non-reacting counterpart, and the peak values occur near $St=0$ which correspond to the long-time average component.

The average streamwise velocity component and velocity vectors for the non-reacting and reacting simulations are compared in Fig. 5. These results show that, for the reacting simulations, the recirculation region is located further downstream compared to the non-reacting case. Moreover, the size of the recirculation region for the reacting case is nearly twice that for the non-reacting one. Visual comparison with the experimental results of Bush and Gutmark[31] indicates that the non-reacting recirculation region is shorter for the numerical simulation compared to the experiments. We attribute this to the two-dimensional character of these results compared to the three-dimensional behavior in the experiments. Shorter recirculation regions were also observed in the two-dimensional results obtained by Erickson et al.[32] The velocity vectors shown in Fig. 5 are in qualitative agreement with the experimental observation of Bush and Gutmark.[31]
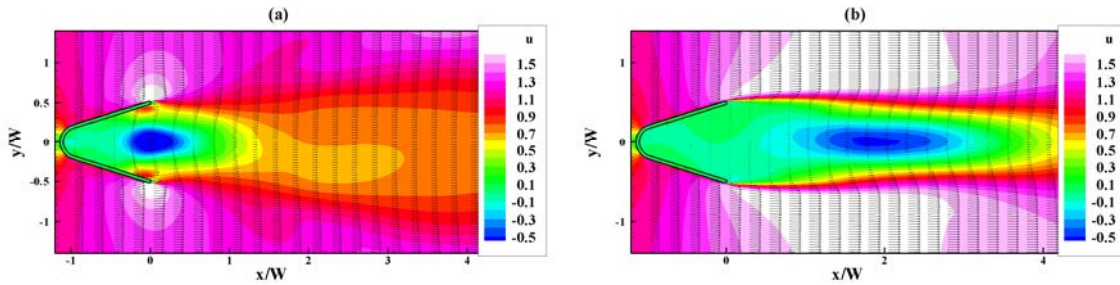

Fig. 5 Average streamwise velocity fields and velocity vectors: (a) non-reacting simulation, (b) reacting simulation.

In order to further validate the present calculations, the average centerline velocity is compared in Fig. 6 with experimental data obtained by Fujii and Eguchi[33] and Sjunesson et al.[34] Although both these studies used bluff-bodies of a different shape compared to the one used in this work, our numerical results for the reacting centerline profile are in good qualitative agreement with the experiments. Comparison of the non-reacting results is consistent with the previous observation that the non-reacting recirculation region is shorter for the numerical simulation. The better agreement that we have observed for the reacting results is attributed to the effect of the chemical heat release on the vorticity field. The volumetric dilatation due to heat release becomes the dominant effect in the redistribution of the vorticity field. This results in reduced vortex stretching effects that are inherent in three dimensional transport of vorticity, leading to a good qualitative agreement between the reacting two dimensional numerical results and the three-dimensional experiments.
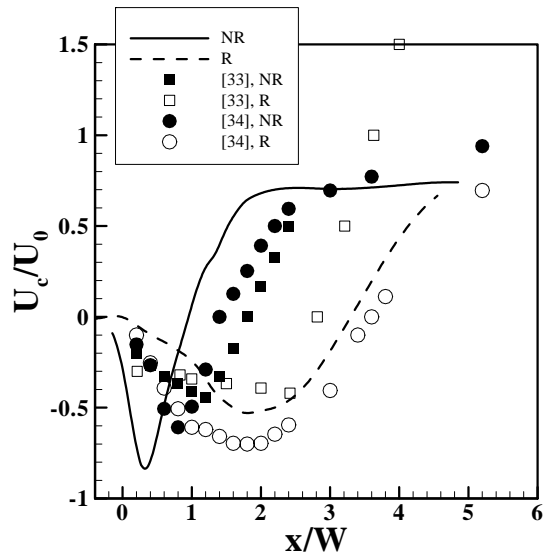
Fig. 6 Comparison of the average centerline velocity profiles between numerical simulations (lines) and experiments (symbols). Both non-reacting (NR) and reacting (R) results are shown. The numbers in brackets correspond to the relevant references.
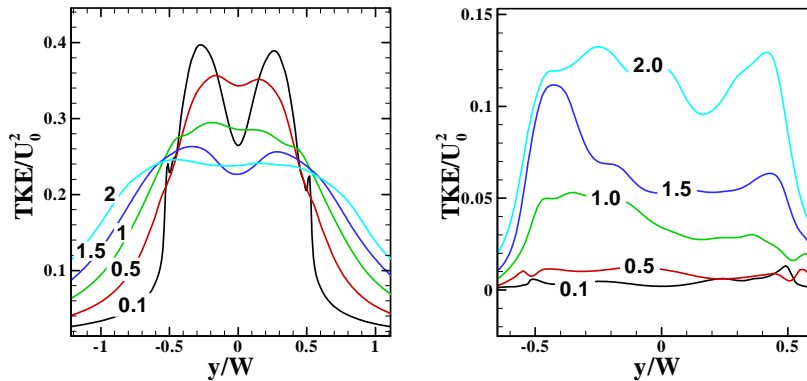
Fig. 7 Normalized turbulent kinetic energy (TKE): (a) non-reacting simulation, (b) reacting simulation. The labels on each profile indicate the streamwise *x/W* location.

Fig. 7 shows the normalized turbulent kinetic energy (TKE) profiles in the wake of the flame holder. Consistent with experimental observations, the TKE values near the centerline (*y=0*) are smaller for the reacting case compared to the non-reacting case. For the locations near the trailing edge, which is located at *x/W=0*, the turbulent levels are much smaller for the numerical results for the reacting case compared to the above experiment. This is attributed to the much larger heat release corresponding to *Φ=1* in the numerical simulation compared to *Φ=0.41* used in the experiments. The smaller TKE values observed here are in agreement to the experimental data obtained by Fujii and Eguchi[33] for similar equivalence ratios.

The weak turbulence intensity near the V-gutter implies small variations in the location of the flame surface. Fig. 8 shows both average and sample instantaneous flame locations. Near the V-gutter, the instantaneous results are almost coincident with the averaged results, while at locations further downstream, the flame surface exhibits large variations.
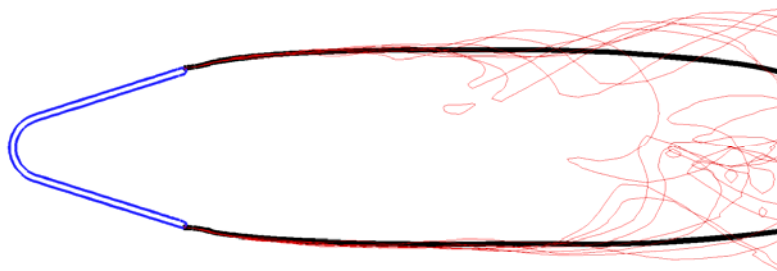

Fig. 8 Average flame location (thick line) and sample instantaneous flame locations (thin lines) at different times.
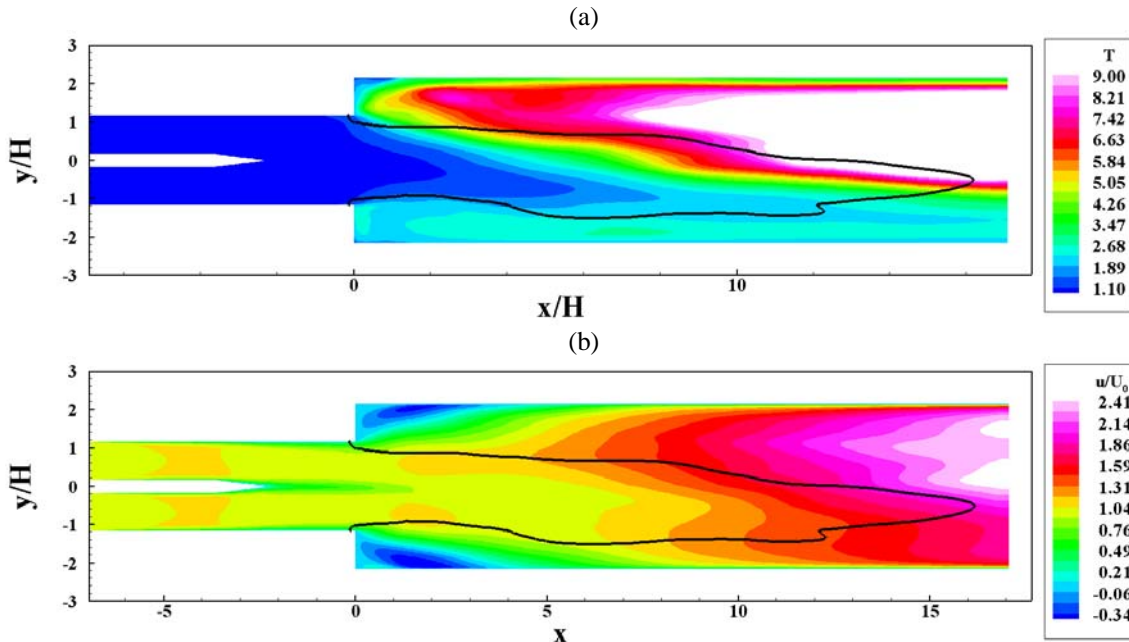
C. Simulation of a Lean Dump Combustor

The Oracles experimental rig[35] is used to test the ability of the level-set/mixture fraction/flamelet formulation to capture the effects of variable equivalence ratios on the flow and combustion characteristics. This experimental configuration has been specifically developed to provide accurate test data for variations in the combustible mixture composition. The setup consists of two fully developed turbulent channel flows that are emerging just before a sudden expansion. The flame is stabilized by the recirculation regions that occur behind each backward facing step. Fig. 9 shows the six-block, two-dimensional computational grid used to perform non-reacting and reacting simulations for this configuration. Each block consists of 75×31 grid points in the computational *x* and *y*-directions, respectively. The computational domain spans 7H upstream of the channel expansion into the combustion chamber. The length of the combustion chamber was set to 20H. This size ensures that the average flame surface is entirely

contained in the computational domain. The Reynolds number in the numerical simulation is set to match the experimental conditions, *Re=25,000*.
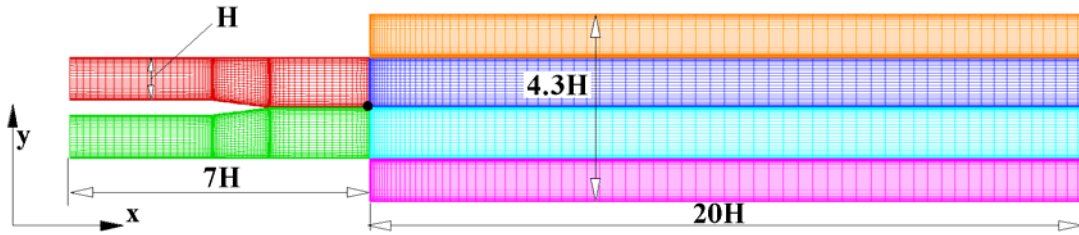
Fig. 9 Computational grid used for the LES of lean dump combustor. The "dot" shows the origin of the physical coordinate system.

This configuration was also used by Duchamp de Lageneste and Pitsch[8] to test the level-set model in their LES procedure for partially-premixed combustion in a low-Mach number flow. Our objective here is to test the ability of a level-set/mixture fraction flamelet approach, coupled with a high-order, fully compressible flow solver, to capture the variable Φ effects on the turbulence chemistry interactions. The results in Fig. 10 are for a reacting simulation with stoichiometric ratios of *0.65* and *0.85* for the lower and upper channels, respectively. For these values of the stoichiometric ratio, the laminar flame velocities, normalized by the bulk flow average velocity, are *0.005* and *0.022*, respectively. Since the turbulent flame velocity is proportional to the laminar value for similar turbulence intensities, based on the model in Eq. (8), this results in larger values for the flame propagation speed on the upper side of the combustion chamber compared to the lower side. The average flame location in Fig. 10 is slanted towards the lower side and is in qualitative agreement with the results of Duchamp de Lageneste and Pitsch.[8] The tip of the flame in the current simulations is located further downstream compared to the results of Duchamp de Lageneste and Pitsch.[8] This is due to a lower stoichiometric ratio that was used in the present study.

(a)

(b)

Fig. 10 Snapshots of normalized time-averaged fields for the lean dump combustor: (a) temperature, (b) streamwise velocity component. The results correspond to a reacting simulation with variable equivalence ratio values: 0.65 for the lower inlet channel and 0.85 for the upper inlet channel.

The mixture on the upper inlet channel corresponds to a fuel-to-oxidizer ratio that is closer to the stoichiometric value compared to the lower channel. This result in larger heat release rates and higher temperatures, in Fig. 10(a),

for the upper side of the combustion chamber compared to the lower side. Since the flow is confined, the volumetric expansion leads to larger streamwise velocities in the upper side compared to the lower side.

In order to determine the effects of heat release on the flow field, the transverse profiles of the axial velocity component for the non-reacting and reacting simulations are compared with the experimental data in Fig. 11. A very good agreement can be observed for the non-reacting results in Fig. 11(a). The reacting results, in Fig. 11(b), also show good agreement and exhibit the flow acceleration observed in Fig. 10(b) for the profiles corresponding to
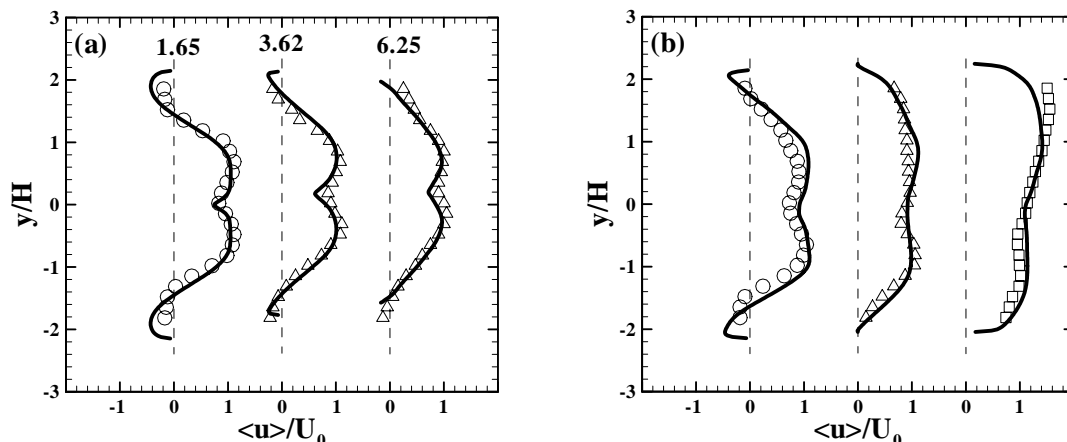
Fig. 11 Comparison of the axial velocity profiles at several locations downstream of the channel expansion: (a) non-reacting simulation and (b) reacting simulation. The vertical dashed lines correspond to zero levels at the corresponding axial locations.

$x/W=1.65$ and $x/W=3.62$. At $x/W=6.25$, the magnitude of the axial velocities on the upper side of the combustion chamber is slightly smaller for the numerical simulation compared to the experiment. The cause for this difference is still under investigation.

IV.   Conclusions

A combined level-set/mixture fraction approach with the capability to predict unsteady, partially-premixed flame configurations is proposed. The compressible flow solver incorporates high-order spatial and time differencing techniques coupled with a matching high-order overset procedure to permit the analysis of realistic problems which usually have very complex geometries. The coupling between chemical reaction and the flow field is achieved through a level-set flamelet formulation for premixed regimes augmented with a mixture fraction approach to account for variations in the equivalence ratio of the combustible mixture.

The above numerical approach is validated through comparisons with experimental data and results from previous numerical studies by other authors. The level-set/flamelet approach is evaluated for the V-gutter flame holder configuration. To our knowledge, this is the first LES simulation for this configuration. The results for the flow field and the flame surface are in good qualitative agreement with the experimental data. The lean, premixed dump combustor is used to test the ability of the combined level-set/mixture fraction approach to capture the variable equivalence ratio for premixed configurations. The good agreement for the velocity field is promising.

Future work will include the comparison of numerical predictions with results from more complex three-dimensional experimental flames, and also the extension of the numerical approach for the prediction of both fuel-rich and fuel-lean, partially-premixed flames.

Acknowledgments

References

[1] Correa, S. M., "Power Generation and Aeropropulsion Gas Turbines: From Combustion Science to Combustion Technology," *Proceedings of the Combustion Institute*, Vol. 27, pp. 1793-1807, 1998.

[2] Williams, F. A., "Turbulent Combustion," *The Mathematics of Combustion*, edited by J. Buckmaster, pp. 97-131, 1985.

[3] Peters, N., *Turbulent Combustion*, Cambridge University Press, 2000.

[4] Nilsson, P., and Bai, X. S., "Effects of Flame Stretch and Wrinkling on CO Formation in Turbulent Premixed Combustion" *Proceedings of the Combustion Institute*, Vol. 29, pp.1873-1879, 2002.

[5] Pitsch, H. and Duchamp de Lageneste, L., "Large-Eddy Simulation of Premixed Turbulent Combustion Using a Level-Set Approach," *Proceedings of the Combustion Institute,* Vol. 29, pp. 2001-2008, 2002.

[6] Pitsch, H., "A Consistent Level Set Formulation for Large-Eddy Simulation of Premixed Turbulent Combustion," *Combustion and Flame*, Vol. 143, pp. 587-598, 2005.

[7] Huang, Y., Sung, H.-G., Hsieh, S.-Y., and Yang, V., "Large-Eddy Simulation of Combustion Dynamics of Lean-Premixed Swirl-Stabilized Combustor," *Journal of Propulsion and Power*, Vol. 19, No. 5, pp. 782, 2003.

[8] Duchamp de Lageneste, L., and Pitsch, H., "Progress in Large-Eddy Simulation of Premixed and Partially-Premixed Turbulent Combustion,", Center for Turbulence Research, Annual Research Briefs, pp. 97-107, 2001.

[9] Lele, S. K., "Compact Finite Differences with Spectral-Like Resolution," *Journal of Computational Physics,* Vol. 103, No. 1, pp. 16-42, 1992.

[10] Shu, C.-W., "Essentially Non-Oscillatory and Weighted Essentially Non-Oscillatory Schemes for Hyperbolic Conservation Laws," ICASE Report No. 97-65, November 1997.

[11] Beam, R. M., and Warming, R. F., "An Implicit Factored Scheme for the Compressible Navier-Stokes Equations," *AIAA Journal*, Vol. 16, No. 4, pp. 393-402, 1978.

[12] Smagorinsky, J., "General Circulation Experiments with the Primitive Equations. I. The Basic Experiment," *Monthly Weather Review,* Vol. 91, No. 3, pp. 99, 1963.

[13] Germano, M., Piomelli, U., Moin, P., and Cabot, W. H., "A Dynamic Subgrid-Scale Viscosity Model," *Physics of Fluids A,* Vol. 3, No. 7, pp. 1760-1765, 1991.

[14] Moin, P., Squires, K., Cabot, W. H., and Lee, S., "A Dynamic Subgrid-Scale Model for Compressible Turbulence and Scalar Transport," *Physics of Fluids A,* Vol. 3, No. 11, pp. 2746-2757, 1991.

[15] Lilly, D.K., "A Proposed Modification of the Germano Subgrid-Scale Closure Model," *Physics of Fluids A,* Vol. 4, pp. 633, 1992.

[16] Safta, C., Alabi, K., and Ladeinde, F., "Comparative Advantages of High-Order Schemes for Subsonic, Transonic, and Supersonic Flows," AIAA Paper 2006-0299, 2006.

[17] Fye, D. J., "Economical Evaluation of Runge-Kutta Formulae," *Mathematics of Computation*, Vol. 20, No. 95, pp. 392-398, 1966.

[18] Kee, R. J., Grcar, J. F., Smooke, M. D., and Miller, J. A., "A Fortran Program for Modeling Steady Laminar One-Dimensional Premixed Flames," Technical Report SAND85-8240, Sandia National Laboratories, 1985.

[19] Lutz, A. E., Kee, R. J., Grcar, J. F., and Rupley, F. M., "OPPDIF: A Fortran Program for Computing Opposed-Flow Diffusion Flames," Technical Report SAND96-8243, Sandia National Laboratories, 1996.

[20] Pitsch, H. and Steiner, H., "Large-Eddy Simulation of a Turbulent Piloted Methane/Air Diffusion Flame (Sandia Flame D)," *Physics of Fluids,* Vol. 12, pp. 2541-2554, 2000.

[21] Harten, A., Engquist, B., Osher, S., and Chakravarthy, S., "Uniformly high order essentially non-oscillatory schemes, III," *Journal of Computational Physics*, Vol. 71, pp. 231-303, 1987.

[22] Shu, C.-W., "Efficient Implementation of Essentially Non-Oscillatory Shock Capturing Schemes," *Journal of Computational Physics*, Vol. 77, pp. 439-471, 1988.

[23] Shu, C.-W., "Efficient Implementation of Essentially Non-Oscillatory Shock Capturing Schemes, II," *Journal of Computational Physics*, Vol. 83, pp. 32-78, 1989.

[24] Sussman, M., Smereka, P., and Osher, S., "A Level Set Approach for Computing Solutions to Incompressible Two-Phase Flows," *Journal of Computational Physics*, Vol. 119, pp. 146-159, 1994.

[25] Russo, G., and Smereka, P., "A Remark on Computing Distance Functions," *Journal of Computational Physics*, Vol. 163, pp. 51-67, 2000.

[26] Safta, C., Alabi, K., Ladeinde, F., and Cai, X., "Level-Set Flamelet/Large-Eddy Simulation of a Premixed Augmentor Flame Holder," AIAA Paper 2006-0156, 2006.

[27] Abdel-Gayed, R. G., Bradley, D., and Lau, A. K. C., "The Straining of Premixed Turbulent Flames," *Proceedings of the Combustion Institute*, Vol. 22, pp. 731-738, 1988.

[28] Cook, A.W., and Riley, J.J., "A Subgrid Model for Equilibrium Chemistry In Turbulent Flows," *Physics of Fluids*, Vol. 6, pp. 2868, 1994.

[29] Kee, R. J., Rupley, F. M., and Miller, J. A., "CHEMKIN-II: A Fortran Chemical Kinetics Package for the Analysis of Gas-Phase Chemical Kinetics," Technical Report SAND89-8009, Sandia National Laboratories, 1989.

[30] Smith, G. P., Golden, D. M., Frenklach, M., Moriarty, N. W., Eiteneer, B., Goldberg, M., Bowman, C. T., Hanson, R. K., Song, S., Gardiner, W. C., Lissianski, V. V., and Qin, Z., http://www.me.berkeley.edu/gri_mech [cited June 10, 2006].

[31] Bush, S.M. and Gutmark, E.J., "Reacting and Non-Reacting Flow Fields of a V-gutter Stabilized Flame," AIAA Paper 2006-807, 2006.

American Institute of Aeronautics and Astronautics

[32] Erickson, R.R., Soteriou, M.C. and Mehta, P.G., "The Influence of Temperature Ratio on the Dynamics of Bluff Body Stabilized Flames," AIAA Paper 2006-753, 2006.

[33] Fujii, S. and Eguchi, K., "A Comparison of Cold and Reacting Flows Around a Bluff-Body Flame Stabilizer," *Journal of Fluids Engineering*, Vol. 103, pp. 328-334, 1981.

[34] Sjunnesson, A., Nelsson, C., and Max, E., "LDA Measurements of Velocity and Turbulence in a Bluff Body Stabilized Flame," *Laser Anemometry*, Vol. 3, pp. 83-90, 1991.

[35] Besson, M., Bruel, P., Champion, J.L., and Deshaies, B., "Inert and Combusting Flows Developing over a Plane Symmetric Expansion: Experimental Analysis of the of the Main Flow Characteristics," AIAA Paper 99-0412, 1999.